AAS 11-056

SMALL BODY LANDING ACCURACY USING IN-SITU NAVIGATION

Shyam Bhaskaran, Sumita Nandi, Stephen Broschart, Mark Wallace, L. Alberto Cangahuala[*], Corwin Olson[†],

Spacecraft landings on small bodies (asteroids and comets) can require target accuracies too stringent to be met using ground-based navigation alone, especially if specific landing site requirements must be met for safety or to meet science goals. In-situ optical observations coupled with onboard navigation processing can meet the tighter accuracy requirements to enable such missions. Recent developments in deep space navigation capability include a self-contained autonomous navigation system (used in flight on three missions) and a landmark tracking system (used experimentally on the Japanese Hayabusa mission). The merging of these two technologies forms a methodology to perform autonomous onboard navigation around small bodies. This paper presents an overview of these systems, as well as the results from Monte Carlo studies to quantify the achievable landing accuracies by using these methods. Sensitivity of the results to variations in spacecraft maneuver execution error, attitude control accuracy and unmodeled forces are examined. Cases for two bodies, a small asteroid and on a mid-size comet, are presented.

INTRODUCTION

Recently, two spacecraft have performed landings on small bodies. The first was the NEAR spacecraft which landed on the asteroid Eros on February 14, 2001 as its final mission event.[1] The second was the Japanese spacecraft Hayabusa which performed several near-touchdowns as well as an unintentional landing on its attempts to retrieve a sample of the asteroid Itokawa in the fall of 2005.[2] In the future, it is expected that in situ analysis and/or sample return missions from asteroids or comets will play a key role in NASAs mission profile, both for its inherent science value as well as adding to our knowledge for use in planetary defense or future manned missions.

From a navigation perspective, landing a spacecraft on small bodies presents special challenges. One of the major decisions is to determine the required navigation delivery performance to the surface. Science-driven requirements aside, at a minimum one must be able to approach the surface safely at a site where there is smooth terrain on the scale of the size

[*] Guidance, Navigation, and Control Section, Jet Propulsion Laboratory, California Institute of Technology, Pasadena, California, MS 230-205, 4800 Oak Grove Dr., Pasadena, CA 91109, Ph: (818)354-0015, Email: Sumita.Nandi@jpl.nasa.gov
[†] a.i. solutions, 10001 Derekwood Lane, Suite 215, Lanham, MD 20706.

of the spacecraft. The minimum dimensions of an acceptable 'smooth site' will be driven by navigation errors accrued en route to the surface. In most cases the number of candidate sites that are larger than these minimum dimensions isn't known until arrival at the small body (with the exception of a few previously imaged bodies such as Eros, Phobos, Deimos, Itokawa, etc.). It's expected that larger small bodies would offer more candidate sites, but in the event that the target body is fixed, the navigation function would have to be refined (through improved maneuver execution, and on-board orbit determination) to reduce the smooth site size threshold and improve the chances of having acceptable options. Assuming that enough candidate sites exist for a given mission, there may be one or two other considerations that may drive navigation performance:

- If the approach to the surface requires timely actions (deployment of hardware, ascent, etc.) that are triggered by an altimeter, it would be prudent to calibrate the altimeter (using radio- metric tracking and optical imagery) by means of a rehearsal run close to the surface of the particular site. Without repeated rehearsals at different sites to more fully understand the effective surface level that the altimeter is sensing, the actual delivery at the surface should take place at the site where the rehearsal took place, which may drive a 'repeatability' requirement on navigation delivery performance.

- In the event that the rehearsal described above perturbs or contaminates the surface, the next best approach would be to attempt to rehearse near, but not exactly at, the final target within the candidate site. As a result, the required dimensions for candidate sites may grow, and the need to avoid the rehearsal area the second time around could result in a tighter navigation delivery performance requirement.

Analysis has shown that standard ground-based navigation techniques can achieve landing accuracies in the tens of meters (1 sigma) range for small bodies (diameters on the order of a few km or less). On very small asteroids or comets, this may not be sufficient. In order to achieve higher accuracy, ground-based navigation will have to be augmented by onboard close loop navigation autonomy. In addition, the latency required to design and implement maneuvers after obtaining the tracking data can range from many hours to days, which contributes to degraded landing accuracies. Two aspects of an onboard navigation system for small body landing applications have been independently demonstrated. The 1st is a general autonomous navigation framework incorporating trajectory propagation, observable and partials generation, maneuver design and targeting, and the executive function driving the system.[3] This was used successfully in flight on three missions: Deep Space 1, Stardust, and Deep Impact. The 2nd aspect is a shape modeling and landmark tracking scheme which can provide accurate line-of-sight vectors to features on the surface that are used as the observables for the navigation process. This system, called OBIRON, was demonstrated as an experimental technique on the ground during the Hayabusa mission on its descents to the surface of Itokawa.[4] The merging of these two form the basis of an autonomous optical navigation system for landing on small bodies.

In this paper, we will provide an overview of the autonomous navigation system, describing the dynamical force models and the error sources affecting a landing scenario. We describe the targeting strategy used to guide a spacecraft to the surface. Finally, we will detail two case studies of landing, one on small asteroid, and another a small comet, and provide the results of Monte Carlo simulations using the autonomous navigation system to quantify the accuracies obtainable.

AUTONOMOUS OPTICAL NAVIGATION

In an autonomous navigation system (referred to from now on as AutoNav), the standard set of functions to perform spacecraft navigation are transferred from the ground to the spacecraft. These functions include obtaining and reducing the observational data, determining the orbit of the spacecraft from this data, and computing correction maneuvers based on the knowledge of the current spacecraft orbit to achieve targeting objectives. An additional function, designing and/or optimizing a planned trajectory, could also be included, but it is not part of the AutoNav system described here; it is assumed that the planned orbit is designed from the ground, and the goal of the system is to follow the design as best it can.

Standard ground-based navigation uses many data types, both radiometric (Doppler and range), interferometric (Delta Differenced One-way Range), and optical. The current AutoNav uses just optical data; this has the advantage of being fairly simple to implement and can be entirely self- contained onboard a spacecraft. The system simulated here was originally designed for the Deep Space 1 mission as a technology demonstration and was used to control the spacecraft through its interplanetary cruise and subsequent flybys of the asteroid Braille and the comet Borrelly. The flyby portion of the code was used on the STARDUST mission on the encounters of asteroid Annefrank and the comet Wild 2, and the full system was used by Deep Impact by the impactor spacecraft to hit the comet Tempel 1 and by the flyby spacecraft to image the impact as it flew by the comet.

Currently, a second generation autonomous navigation system is being developed at JPL which builds on the DS1/DI system, and will include attitude control functions as well as navigation.[5] This is especially important for very close proximity operations such as landing or touch and go for sample collections on small bodies where a tight coupling between the spacecraft translational and rotational motion is necessary. The system also includes the OBIRON landmark tracking capability as its primary data for navigation. This system, called AutoGNC, is at a TRL 5 level and has been demonstrated in a fully dynamic simulation to be able to control a spacecraft towards landing on comets and asteroids.

The full AutoGNC is built on C++ and VML and is intended to very near flight code. Our purpose, however, is to examine the capability of the algorithms used by the navigation portions of AutoGNC to perform a landing on an asteroid or comet. We do this by the use of Monte Carlo simulations, with realistic models of the forces that act on the spacecraft and the associated error sources. Since AutoGNC runs in near real-time, Monte Carlo simulations are impractical to run. We therefore have MATLAB version of the algorithms which perform the navigation functions that we can use for this purpose. These algorithms are virtually unchanged from the DS1/DI AutoNav system, and so we continue to use this term for the remainder of this paper. A detailed description of the AutoNav system can be found in reference 6.

REFERENCE TRAJECTORY

Two scenarios were used to test the AutoNav capability; the first is a landing on a fairly small asteroid, and the second is landing on a slightly larger comet which is fairly representative of the size of short period comets visited by spacecraft thus far. Since the goal of AutoNav is to guide the spacecraft along a pre-described path, reference trajectories were designed for each scenario which took the spacecraft from some altitude to landing. These reference trajectories have deterministic and statistical maneuvers, both of which will be

adjusted by AutoNav using its onboard orbit deter- mination to make course corretions. The following subsections describe the reference trajectories used for the landing simulations.

Asteroid Landing

The body used for the asteroid reference trajectory was an 760 x 680 x 500 meter radii triaxial ellipsoid modeled as having a uniform density of 1.14 g/cm^2. This body is about twice the size of Ikotawa and one third the size of Eros. In addition to its small mass (gravitational constant of 1.04 x 10−7 km^3/s^2), it rotates

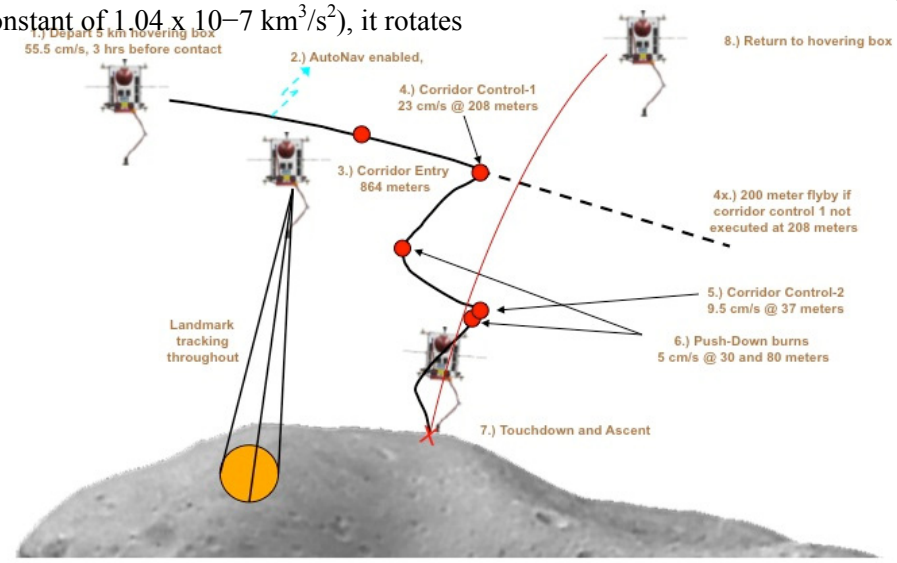

Figure 1. Asteroid Descent Trajectory Illustration

on its axis once every 3.6 hours. As a result, small errors in the timing of contact can translate into very large errors in the position. In addition, maintaining a near-zero horizontal contact velocity is a particular challenge. As a stressing case, the reference trajectory was targeted to contact the surface of the asteroid at the tip of its long axis with a vertical velocity of 20 cm/s.

The trajectory begins in an equatorial station-keeping box positioned so that the landing trajectory remains above the sun-lit portion of asteroid during the entire trajectory. 3 hours before contact, the spacecraft executes a 55.5 cm/s burn to put it on a close flyby trajectory. If no further maneuvers are executed, the spacecraft will fly past the asteroid's surface at an altitude of 200 meters. The subsequent maneuvers are all designed to keep the targeted contact site within the field of view of a nadir-looking camera (green lines in Figure 1) while below 860 meters. This necessitates a pair of "corridor control burns" in the asteroid anti-rotation direction, that is, roughly parallel to the surface of the comet. These burns are executed 21 and 3 minutes before contact. The other two burns in the trajectory are "push down burns," designed to provide a bias in the statistical maneuvers. These 5 cm/s maneuvers are required to ensure that statistical maneuvers do not result in thruster plume impingement on the asteroid surface, risking contamination of the target landing site. The first occurs between the two corridor control burns, and the second occurs only 2.5 minutes before contact. Finally, two statistical maneuvers are added, one between the orbit departure and 1st corridor control, and one right before touchdown. The former helps control the position error at landing while the latter controls the velocity dispersion. The details of the maneuvers are listed in Table 1.

Table 1. Asteroid Landing Maneuver Schedule

Maneuver	Time to Landing	Deterministic Magnitude (cm/s)
Orbit Departure	2:50:34 hr	55.5
Clean-up 1	1:34:17 hr	0
Corridor Control 1 (CC-1)	21:09 min	23.0
Push Down 1 (PD-1)	7:40	5
Corridor Control 2 (CC-2)	3:18	9.5
Push Down 2 (PD-2)	2:31	5
Cleanup 2	31 sec	0

Comet Landing

For the comet landing scenario, we used a realistic comet model based on observations of Tempel 1 by the Deep Impact mission. The shape model for Tempel 1 (see Reference 9[7]) is used here to define the comet surface for this scenario (Figure 2). This shape model measures roughly 7.4 x 6.2 x 5.4 km with an equivalent spherical radius of 3.0 km.

The touchdown target for the spacecraft center of mass is 4 m above the surface of the comet model at -29.1 deg latitude and 9.5 deg longitude with respect to a body-fixed frame. This target was selected primarily because of the locally smooth terrain features seen by Deep Impact and desirable lighting geometry during the descent.

A point mass model is used to model the gravitational potential of the comet. Using the shape described above and a estimated bulk density of 0.6 g/cm^3, the gravitational parameter for this model is 4.479 x 10−6 km3/s^2.

Tempel 1 is assumed to be in uniform rotation with a 40.7 hr sidereal period around a rotation pole that is oriented at 78 deg declination and 5 deg right ascension in the Earth Mean Equator of J2000 (EME2000) inertial coodinate frame. Thus, the surface at the targeted touchdown position moves eastward at 8 cm/s with respect to the comet center of mass.

For this scenario, the comet is modeled as being 3.6 AU from the Sun at the epoch of descent. This range is consistent with greatly reduced comet outgassing activity that is somewhat random in nature. Also, a descent to the surface of a comet would not likely be attempted until outgassing activity has diminished. Thus, for the modeling of the nominal trajectory, acceleration on the spacecraft due to comet outgassing is not included.

The spacecraft considered for this scenario is assumed to have a mass of 2400 kg and an effective mass-to-area ratio of 28.1 (for the purpose of solar radiation pressure calculation). In the baseline trajectory design, all maneuvers are assumed to be impulsive.

An illustration of the baseline trajectory is shown in Figure 3. The baseline trajectory begins with the spacecraft 120 km from the comet center of mass on a hyperbolic flyby trajectory (1.18 m/s speed) with a close approach safely above the comet surface. Approximately 26 hours later, the spacecraft executes the 1.38 m/s “drop burn” at 500 m altitude, which puts the spacecraft on a surface intersecting trajectory. If the drop burn is not executed, the

spacecraft will safely flyby the comet. The spacecraft then moves toward the surface of the comet for 23 minutes until the 0.81 m/s "braking burn #1" is executed at 110 meters altitude. See Table 2 for a list of the deterministic and statistical burns for this scenario. Touchdown occurs 4.5 minutes later, which is 33.3 minutes after the execution of the "drop burn" and 27 hours after the trajectory begins at 120 km.

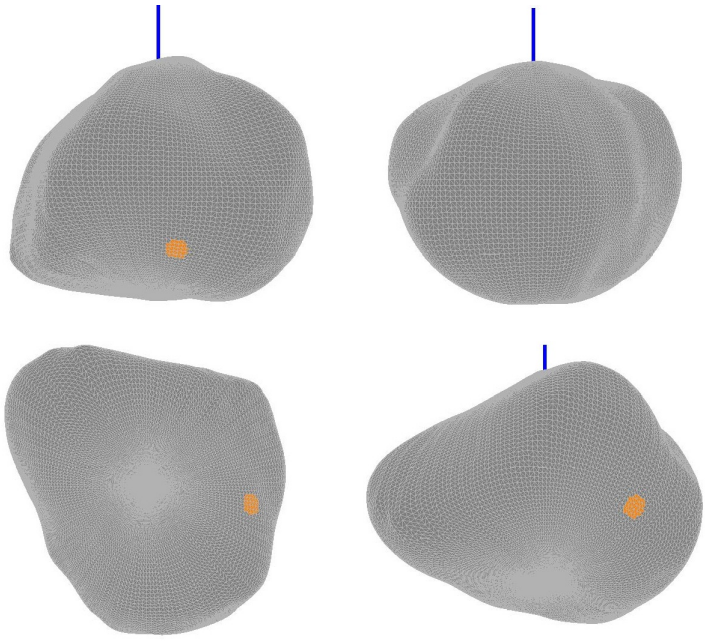

Figure 2. Polyhedral representation of the Tempel 1 shape model (Reference 7) viewed along each principal axis and from an oblique angle. The north pole is indicated by the heavy blue line. The targeting landing site is highlighted in orange.

Table 2. Comet Landing Maneuver Schedule

Maneuver	Time to Landing	Deterministic Magnitude (cm/s)
Drop Burn	32:40 min	138
Clean-up 1	28:00 min	0
Clean-up 2	19:20 min	0
Braking Burn 1	10:07 min	81
Clean-up 2	7:00 min	0
Braking Burn 2	4:33 min	24

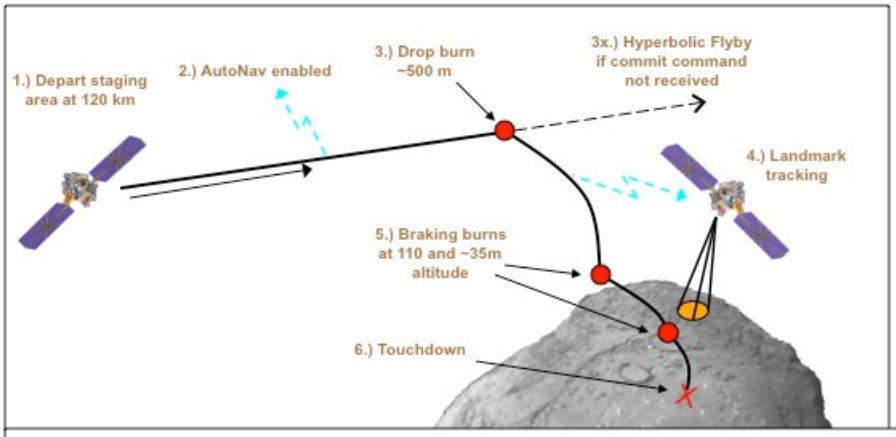

Figure 3. Comet Touch-and-Go Trajectory Illustration

MONTE CARLO SIMULATIONS

If the dynamic equations used in the filter precisely modeled the true forces acting on the spacecraft, and the errors in the models and data were truly random and Gaussian, then the covariance obtained after filtering would accurately represent the statistics of the estimated values. This is not the case however, as we have deliberately used a reduced set of dynamics to keep the algorithm simple and fast (for example, truncating the gravity field), and we know that maneuver execution errors are not Gaussian. For this reason, Monte Carlo simulations are needed to assess the ability of AutoNav to target a landing spot on the surface. For the simulations, a "truth" model of the trajectory, spacecraft attitude, and observations are generated and provided to the filter. For a given run, the truth model represents a random sampling of the error sources which affect that model. Five-hundred runs are performed, and the results are evaluated by determining where the "truth" trajectories in each run landed on the surface. In the next two sections, the details of the error sources and simulation results for each of the landing cases are described.

Asteroid Landing

In the asteroid landing scenario, AutoNav is started 1 hour before orbit departure burn (see Table 1). For targeting, the first 6 maneuvers target the reference trajectory position at the time of the subsequent maneuver; the last maneuver was targeted at the cartesian target landing location in body-fixed coordinates, at the specified landing time. For deterministic maneuvers, the targeting algorithm will adjust the design values given in Table 1 whereas it will start from 0 for the statistical maneuvers. Images are taken starting at a rate of one image every 5 minutes, increasing to one image every 30 seconds after CC-1, and finally at 10 second intervals after PD-1. In Table 3, the parameters which describe the error sources which the simulation samples is listed. Table 4 lists the parameters used by the kinematic and dynamic filters in AutoNav.

For the gravity field, the truth model used a full 12x12 field representing a uniform density triaxial ellipsoid, with a GM value of 1.04x10−7 km^3/s^2. The dynamic model used in the AutoNav filter, however, used a field truncated to degree and order 4. Furthermore, for sampling gravity field errors in the truth model, the following formula was used. First, compute

the average amplitude of the coefficients by degree. Then, apply the average value per degree as the uncertainty on the coefficients of that degree and order, multiplied by a scale factor: The scale factors chosen were 10%, 25%, 50%, and 75% for degrees 1-4. Beyond this, since the onboard filter does not model the field, the true field is used as is, without applying any random variations.

One error source which tends to dominate in small body landing situations are the execution errors from the maneuvers. In the truth simulation, as each maneuver is implemented, an error is applied whose values are sampled using the Gates model representation for maneuver errors.[8] The parameters in the Gates model are fixed and proportional errors for the magnitude as well as well as the direction of the burn. Table 5 lists the Gates model values used in the simulations.

The results of a 500 sample Monte Carlo simulation are shown in the following figures. Figure 4 shows the scatter of landing locations in a topocentric coordinate system, with the origin being the targeted landing spot (and indicated by the red dot). Note that the scatter is very tight, with 100% of the samples being under 4 m in radius. Figures 5 and 6 show the corresponding scatter in the landing velocities, also in a topocentric frame, with the former being a slice of the samples in a horizontal direction and the latter being in the vertical direction. Since the design trajectory landed with 0 horizontal velocity, the scatter in this frame is centered at 0, with the maximum dispersion being about 2 cm/s. The design trajectory had a 15 cm/s component in the vertical direction, so the scatter in this plot is centered around 15 cm/s. Once again, the maximum dispersion is less than 2 cm/s.

Table 3. Simulation Error Parameters

Parameter	Error Sampling (1s)	Comment
Position	5 km	Assume Spherical Gaussian Distribution
Velocity	10 m/s	Assume Spherical Gaussian Distribution
Solar Pressure	5%	
Small Forces	1 mm/s	Assume Spherical Gaussian Distribution, event every 20 min
Attitude	0.7 mrad	Random distribution
Gravity Field		See Text

Table 4. Filter Parameters

Parameter	Error Sampling (1s)	Comment
Position	10 m	Assume Spherical Gaussian Distribution
Velocity	5 mm/s	Assume Spherical Gaussian Distribution
Observable Data Weight	0.25 pixels	For Kinematic filter
Observable Data Weight		Dynamic filter uses output from kinematic filter

Table 5. Gates Maneuver Execution Error Model Parameters

Parameter	Error Sampling (1s)
Fixed magnitude	4.3 mm/s
Proportional magnitude	10%
Fixed direction	4 mm/s
Proportional direction	3.1%

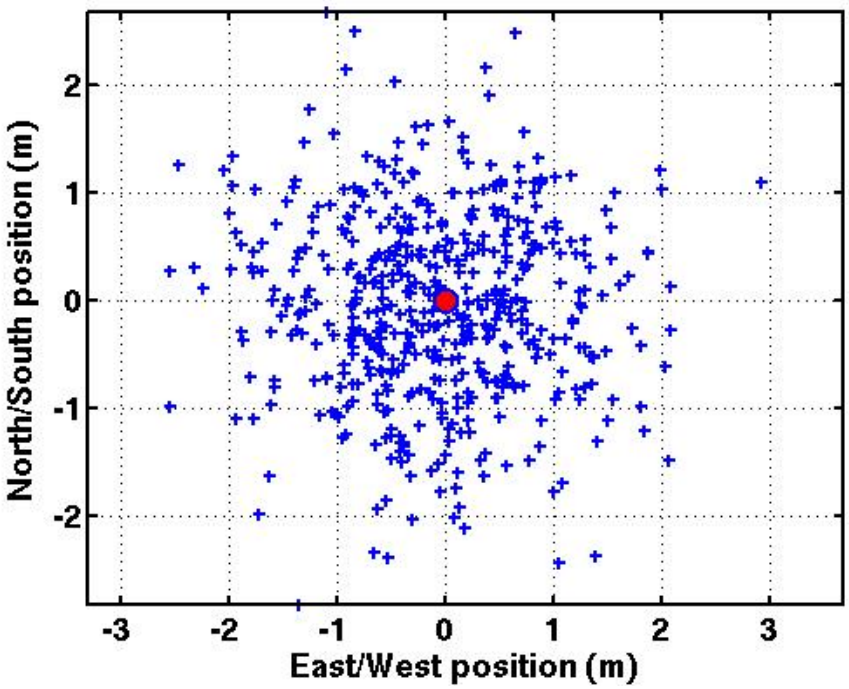

Figure 4. Asteroid Landing Position Dispersionsin Horizontal Plane

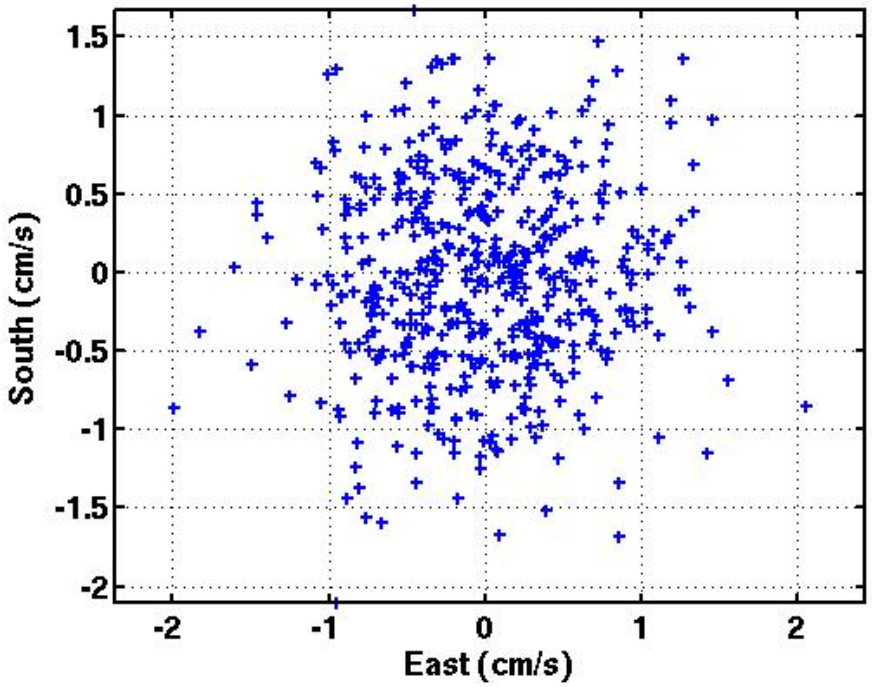

Figure 5. Asteroid Landing Horizontal Velocity Dispersion

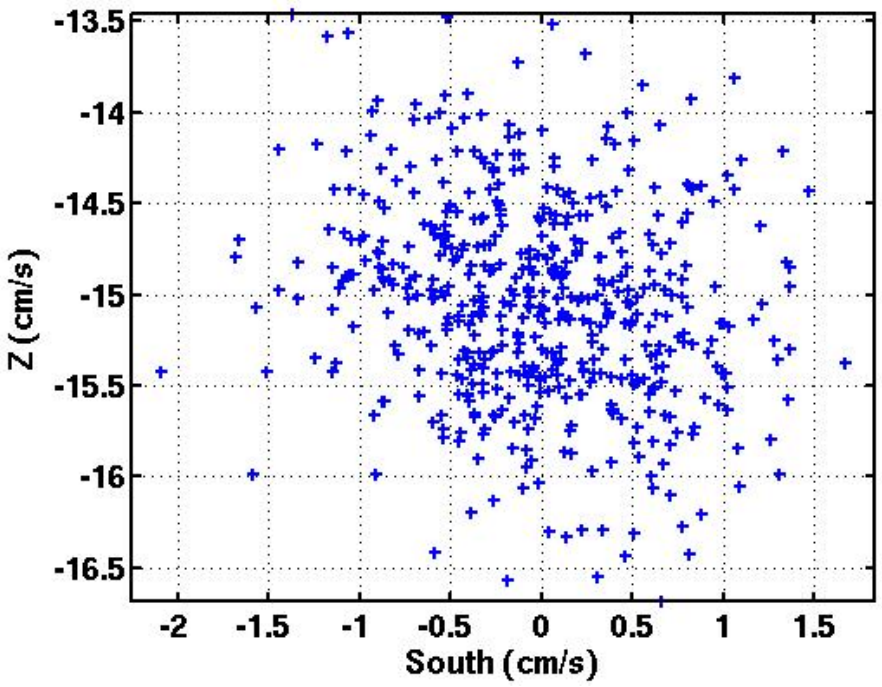

Figure 6. Asteroid Landing Vertical Velocity Dispersion

Comet Landing

For the comet landing scenario, AutoNav is seeded with states having an error distribution that is spherical in all six coordinates at 3.5 hours prior to touch-and-go (TAG). Each state is propagated through three deterministic (a drop burn and two braking burns) and two statistical maneuvers, within 30 minutes of TAG. Each maneuver is computed by AutoNav to target a specific latitude and longitude at 5 m above the comets nominal surface, propagating through future deterministic maneuvers. The maneuvers were simulated with a Gates model error distribution with 0.5 % proportional magnitude error and 1% proportional direction error (see Table 7). Fixed errors were considered to be insignificant for the thruster system being considered. The gravity of the comet is modeled with a GM of 4.479x10−6 km^3/s^2 and 4x4 field from a shape model. The errors associated with the gravity field were assessed by using a model in the filter that was different from the truth model for order 1 through 4 components of 10%, 25%, 50% and 75%, respectively. Simulation errors are summarized in Table 6. Images are taken each hour up to one hour prior to the first maneuver, each three minutes up to the first maneuver, and finally each 30 seconds after the first maneuver up through TAG.

Dispersion results at the targeted altitude are shown in Figures 7 to 9 for the baseline simulation scenario. Small force disturbances and attitude errors were not modeled in the baseline simulation, but the sensitivity to those factors is tested in separate simulations which perturb the baseline simulation with the addition of the error source of interest. Because the landing dispersion is heavily dependent on the assumed maneuver execution error, a case which doubles the maneuver execution error was also studied. Doubling the maneuver

execution error causes a 35% increase in the position and velocity landing dispersions. Table 8 shows the results of each of the sensitivity studies.

Table 6. Comet TAG Simulation Error Parameters

Parameter	Error Sampling (1s)	Comment
Position	5 km	Assume Spherical Gaussian Distribution
Velocity	10 m/s	Assume Spherical Gaussian Distribution
Solar Pressure	5%	81 m^2 area
Gravity Field	See Text	4x4 field
Observable Accuracy	0.25 pixels	
Maneuver Magnitude	0.5 %	No fixed error
Maneuver Direction	0.9 %	No fixed error

Table 7. Comet Maneuver Statistics

Maneuver	Reference Deterministic Magnitude (cm/s)	Mean Magnitude (cm/s)	99% magnitude (cm/s)
Drop Burn	138	139.3	214.1
Clean-up 1	0	30.3	71.8
Clean-up 2	0	5.7	14.1
Braking Burn 1	81	81.1	89.3
Clean-up 2	0	2.6	5.7
Braking Burn 2	24	24.3	26.0
Total		283.4	374.7

Table 8. Comet Perturbation Case Results

Parameter	Parameter Perturbation	Position Dispersion Increase (%)	Velocity Dispersion Increase (%) South-East	Velocity Dispersion Increase (%) South-Vertical
Small Force Disturbance	1 mm/s each 20 min	5.2	9.1	4.8
Maneuver Execution Error	1% Magnitude, 1.8% Direction (double nominal)	38	35	36
Attitude Error	0.7 mrad	4.0	8.9	9.4

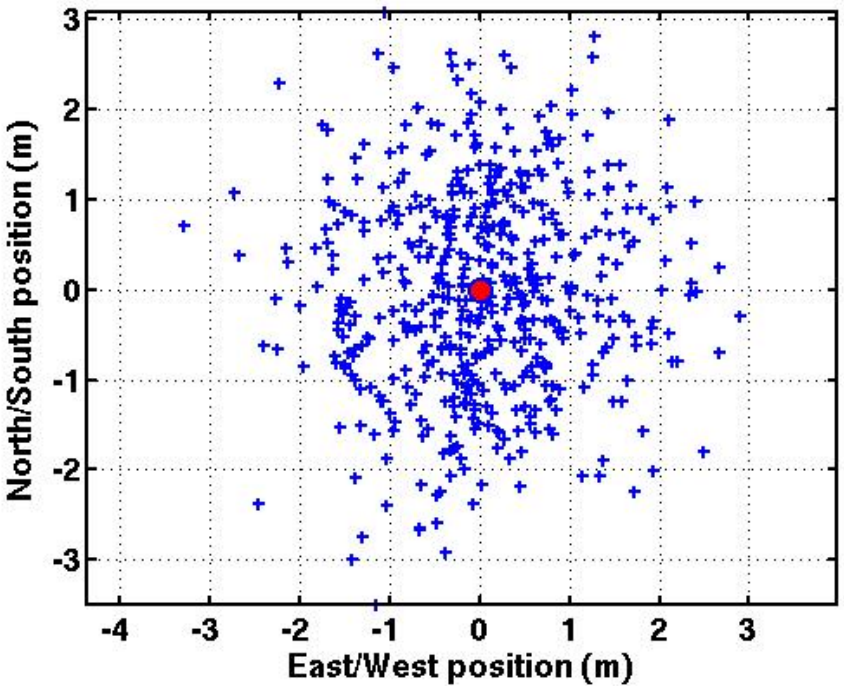

Figure 7. Comet Touch-and-go Horizontal Position Dispersion

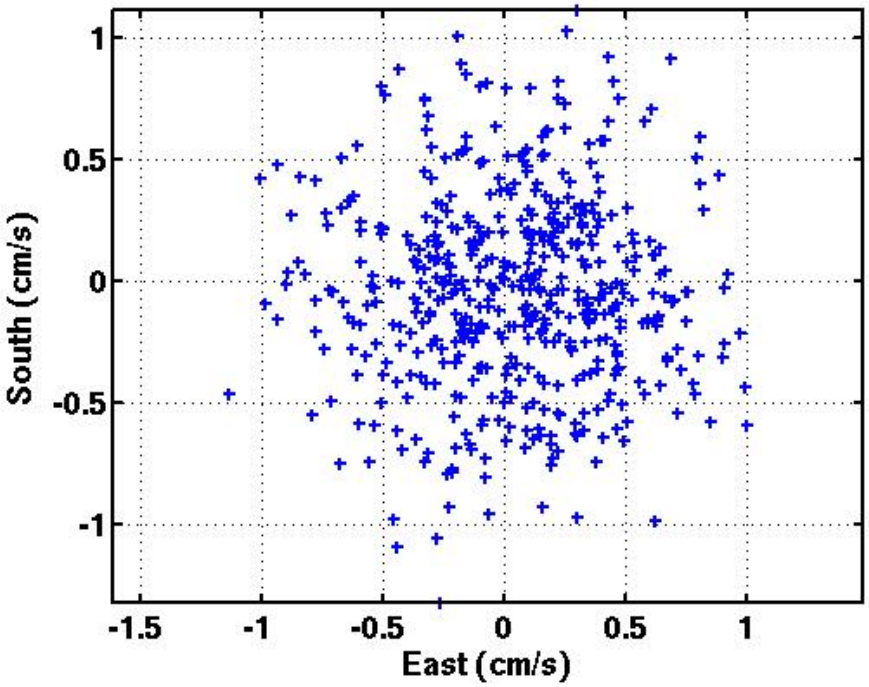

Figure 8. Comet Touch-and-go Horizontal Velocity Dispersion

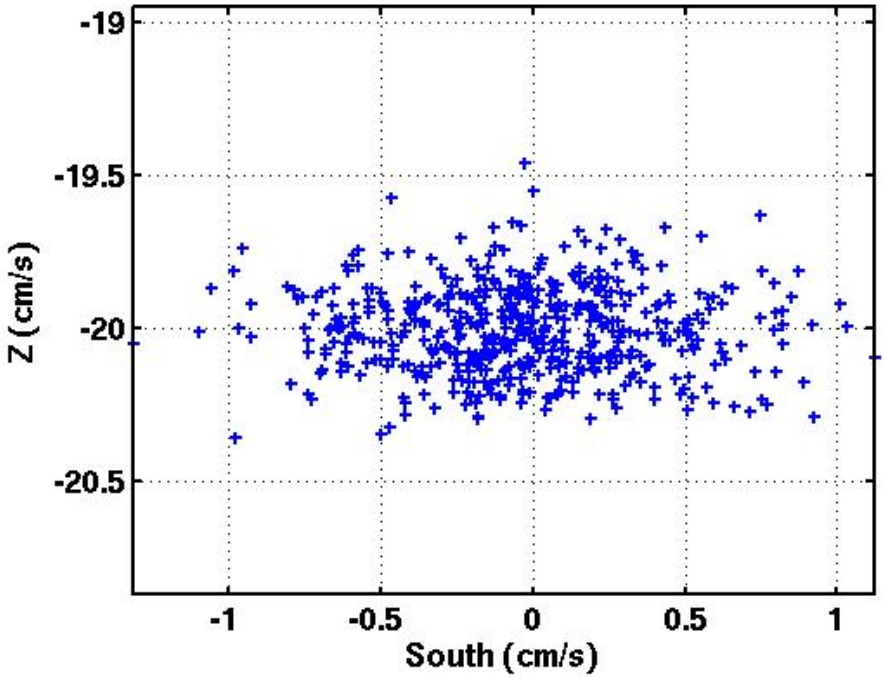

Figure 9. Comet Touch-and-go Vertical Velocity Dispersion

CONCLUSIONS

The results of this study show that landing accuracies under 10 m on small bodies is both feasible and realistic if the spacecraft has an onboard AutoNav capability. Even when the onboard system has a reduced set of dynamic models, the rapid turnaround enabled by the system allows it to correct for a realistic set of perturbations and guide the spacecraft accurately to its intended target. Such a capability is not realizable when the ground is in the loop due to many limitations, including the round-trip light time delay. Furthermore, the use of onboard navigation autonomy has already been proven on three separate missions; the addition of the landmark tracking capability represented by OBIRON is an evolutionary, rather than revolutionary step. For future missions which intend to land on small bodies, the capability to have a very small landing footprint presents an opportunity to greatly enhance the robustness and science return on these missions, with a relatively modest investment in new technologies.

ACKNOWLEDGEMENT

This research was carried out at the Jet Propulsion Laboratory, California Institute of Technology, under a contract with NASA.

REFERENCES

[1] P.Antreasian, S.Chesley, J.Miller, J.Bordi and B.Williams,"The Design and Navigation of the NEAR Shoemaker Landing on Eros," AAS/AIAA Astrodynamics Specialists Conference, July 2001. Paper AAS 01-372.J.L. Doe

and J.Q. Public, "The Parameterization of the Rotation Matrix using Redundant Attitude Coordinates." *Nonlinear Dynamics*. Vol. 32, No. 3, 2005, pp. 71–92.

[2] H. Yano, T. Kubota, H. Miyamoto, T. Okado, D. Scheeres, Y. Takagi, K. Yoshida, M. Abe, S. Abe, O. Barnouin-Jha, A. Fujiwara, S. Hasagawa, T. Hashimoto, M. Ishiguro, Kato, J. Kawaguch, T. Mukai, J. Saito, S. Sasaki, and M. Yoshikawa, "Touchdown of the Hayabusa spacecraft at the Muses Sea on Itokawa," Science, No. 5778, 2006, pp. 1350–1353.

[3] J. E. Riedel, S. Bhaskaran, and S. P. Synnott, "The New Millennium DS-1 Autonomous Navigation System," NASA Tech Brief NPO-19939, No. 1, January 1997.

[4] R. Gaskell, O. Barnouin-Jha, D. J. Scheeres, A. S. Konopliv, T. Mukai, S. Abe, J. Saito, M. Ishiguro, T. Kubota, T.Hashimoto, J. Kawaguchi, M. Yoshikawa, K. Shirakawa, T. Kominato, N. Hirata, and H. Demura, "Characterizing and Navigating Small Bodies with Imaging Data," Meteoritics and Planetary Science, Vol. 43, Sept. 2008, pp. 1049–1061.

[5] J. Riedel, T. Wang, R. Werner, A. Vaughan, D. Myers, N. Mastrodemos, G. Huntington, C. Grasso, R. Gaskell, and D. Bayard, "Configuring the Deep Impact AutoNav System for Lunar, Comet, and Mars Landing," AAS/AIAA Astrodynamics Specialist Conference, August 2008. Paper AIAA-2008-6940.

[6] S. Bhaskaran, S. Nandi, S. Broschart, M. Wallace, L. A. Cangahuala and C. Olson, "Small Body Landings using Autonomous Onboard Optical Navigation", Paper presented at the George Born Symposium, Boulder, CO, May 13-14, 2010.

[7] P. Thomas, J. Veverka, M. Belton, A. Hidy, M. A'Hearn, T. Farnham, O. Groussin, J. Li, L. McFadden, J. Sunshine, D. Wellnitz, C. Lisse, P. Schultz, K. Meech, and A. Delamere, "The Shape, Topography, and Geology of Tempel 1 from Deep Impact Observations," Icarus, Vol. 191, No. 2, Supplement 1, 2007, pp. 51 – 62.

[8] C. R. Gates, "A Simplified Model of Midcourse Maneuver Execution Errors," JPL-Technical Report 32-504, October 15, 1963.